INTERNATIONAL JOURNAL OF SMART AND NANO MATERIALS
2019, VOL. 10, NO. 3, 177–204
https://doi.org/10.1080/19475411.2019.1631899

Taylor & Francis
Taylor & Francis Group

ARTICLE

Advanced 4D-bioprinting technologies for brain tissue modeling and study

Timothy J. Esworthy[a], Shida Miao[a], Se-Jun Lee[a], Xuan Zhou[a], Haitao Cui[a], Yi Y. Zuo[b] and Lijie Grace Zhang[a,c,d,e]

[a]Department of Mechanical and Aerospace Engineering, The George Washington University, Washington, DC, USA; [b]Department of Mechanical Engineering, University of Hawaii at Manoa, Honolulu, HI, USA; [c]Department of Medicine, The George Washington University, Washington, DC, USA; [d]Department of Biomedical Engineering, The George Washington University, Washington, DC, USA; [e]Department of Electrical and Computer Engineering, The George Washington University, Washington, DC, USA

ABSTRACT

Although the process by which the cortical tissues of the brain fold has been the subject of considerable study and debate over the past few decades, a single mechanistic description of the phenomenon has yet to be fully accepted. Rather, two competing explanations of cortical folding have arisen in recent years; known as the axonal tension and the differential tangential expansion models. In the present review, these two models are introduced by analyzing the computational, theoretical, materials-based, and cell studies which have yielded them. Then Four-dimensional bioprinting is presented as a powerful technology which can not only be used to test both models of cortical folding *de novo*, but can also be used to explore the reciprocal effects that folding associated mechanical stresses may have on neural development. Therein, the fabrication of 'smart' tissue models which can accurately simulate the *in vivo* folding process and recapitulate physiologically relevant stresses are introduced. We also provide a general description of both cortical neurobiology as well as the cellular basis of cortical folding. Our discussion also entails an overview of both 3D and 4D bioprinting technologies, as well as a brief commentary on recent advancements in printed central nervous system tissue engineering.

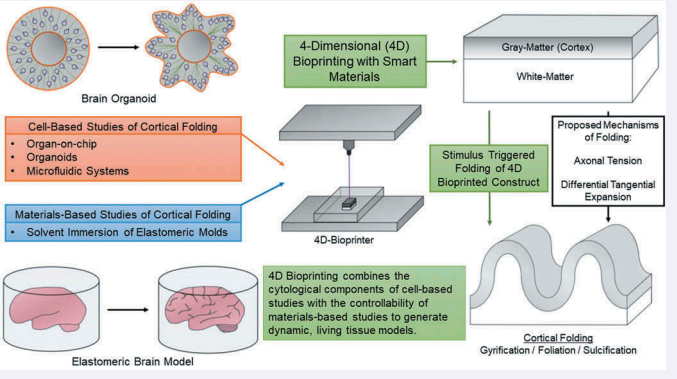

ARTICLE HISTORY
Received 22 October 2018
Accepted 10 June 2019

KEYWORDS
4D bioprinting; smart materials; brain; cortical folding; gyrification

CONTACT Lijie Grace Zhang lgzhang@email.gwu.edu Department of Mechanical and Aerospace Engineering, The George Washington University, Washington, DC 20052, USA

1. Introduction

The process by which the cortical tissues of the brain enfold in order to form its wrinkled topology has been the subject of extensive study over the past several decades, yet the exact mechanisms which guide this process remain poorly understood. However, it has been found that the manner in which the cortical tissues fold has a critical effect on conventional neurological development. Therein, aberrant folding has been shown to be correlated with the presentation of certain neurological disorders, such as autism, schizophrenia, and some forms of psychosis [1–6]. Both theoretical and computation models have been proposed in an attempt to give a general description of the mechanics of neural tissue folding; however, a unified mechanism has yet to be fully accepted [7–14]. For a more comprehensive discussion of the various proposed computational models of cortical folding, the reader is referred to the works of Bayly *et al.* (2014) and Striedter *et al.* (2015) [15,16]. Recently, abiotic materials-based studies have challenged, verified, and extended existing theoretical models of cortical folding [17,18]. However, since these materials-based studies do not incorporate living cells, they largely cannot account for the potential unforeseen effects that cells and their physiological processes might have on the mechanics of tissue development such as stiffening and folding [14,19–21]. Therefore, these materials-based studies arguably best serve as a general description of the likely mechanisms which underlie cortical folding, rather than a fully comprehensive account of the phenomenon as a whole.

Living neural tissue is heterogenous in cytological composition and is thereby variable with regard to its localized mechanical properties. Cell and tissue engineering studies have found that the *in vivo* process of cortical folding is largely related to the spatial distribution and patterning of certain cell types within the cortical and subcortical tissues. The expression levels of specific neurotrophic factors and the localized forces that both cell migration and proliferation impact on the mechanical characteristics of the developing tissue also play crucial roles in the initiation of the folding process [14,22–27]. As a general trend, the primary focus of these types of studies has been on establishing a unidirectional, causative relationship between cellular processes, such as the rate of proliferation at a given location within a tissue, and the resultant mechanical stresses they generate being the driving force behind the initiation of cortical folding. In this way, these studies do not appear to consider the potential for a positive feedback relationship between the forces cortical cells generate to initiate the folding cascade, and the reciprocal role the mechanical stretching and compressing of the buckling tissue may play in reinforcing neural-cell fate commitment and organization *via* mechanosensing mechanisms. If there is indeed a reciprocal relationship between cell-initiated tissue folding and the secondary effects these stresses confer on neural-cell processes, then studying this relationship may provide critical insights into how differences between folding patterns relate to normal and aberrant neurological functioning. Further exploration of this complex interplay between folding associated stresses, neural-cell development, and network establishment seemingly demands a model system which incorporates the spatial-mechanical control of materials-based studies with the true-to-nature functionality of cell-based models. Namely, in order to obtain a more comprehensive and physiologically relevant model of the neural-developmental process of cortical tissue folding, future studies should likely focus on

using models constructed from cell-laden 'smart'- materials. These so-called smart materials can artificially simulate the mechanical stresses associated with cortical folding in order to observe the potential effects these forces might have on neural-cell maturation and functionality. By extension, the folding patterns of these smart-neural tissue constructs can be tuned and modified in order to further study the etiology of various neurological diseases at a biomechanical level. Fortunately, recent advancements in three-dimensional (3D) and four-dimensional (4D) bioprinting may offer a promising means by which to reliably fabricate these biomimetic, smart-models of living neural tissues [28–43].

4D bioprinting is a cutting-edge additive manufacturing technology which has an intrinsic capability to fabricate *de novo* living tissue constructs which can be made to change in various mechanical or physio-spatial aspects when subjected to predetermined stimuli or trigger sources [44]. Moreover, 4D-bioprinting techniques can be used to place both living cells and growth factors in highly ordered, biomimetic motifs which can undergo physiologically relevant transformations which accurately simulate developmental processes, such as tissue stretching, compressing, or the shifting of the biomaterial's modulus. In this context, the fourth dimension in '4D bioprinting' refers to the element of time which one or more of a 3D printed object's physical attributes are functionally dependent upon. Put another way, a 4D-bioprinted construct's conformation or physical characteristics vary through time as a consequence of a given triggering mechanism or stimulus. In this way, these complex 4D objects can be designed in such a manner which they exhibit an inherent 'self-assembly' attribute, whereby a construct will change in shape, conformation, or consistency immediately following the printing process. The feature of self-assembly that some 4D-bioprinted objects display arises from physically based information or modular cues which are directly incorporated into the construct's design and the formulation of the printing material. Wherein these internally based cues guide the construct through the dynamic transformation process once the printing is completed and an external stimulus is enacted [36].

In contrast to the rapidly occurring physical transformations undergone by self-assembly enabled 4D-printed constructs, most bioprinted constructs used to model the development of various tissue structures require the transformation process to occur at more gradual, physiologically relevant timescales. As such, shape memory polymers (SMPs) are particularly useful biomaterials which can be printed into a given conformation and can be reversibly transformed between various temporary states as a function of selective triggering mechanisms [36]. Much in the same way that self-assembly enabled constructs bear physically encoded information which guides the transformative process, SMPs and other triggerable constructs rely on physical (or chemical) modalities inherent to their design and formulation to actuate desired physical transformations as well. The key difference between constructs which are self-assembly enabled and those which are not, is that non-self-assembly objects can maintain a post-print conformation for an extended period of time before the transformative trigger is enacted. Thereby, cells can easily be seeded onto non-self-assembly constructs before the transformation process occurs. This, in turn, affords researchers the opportunity to study the effects that the mechanical stresses generated by the transformation process have on cellular growth and behavior.

The manner by which a SMP or other 4D-bioprinted construct can be triggered to undergo a desired physical change is largely contingent on the chemical nature of the biomaterial. Typically, exogenous trigger mechanisms for 4D-bioprinted constructs involve thermal induction, chemical or solvent immersion, electrical stimulation, or light induction [36]. Therein, the speed at which a 4D-bioprinted construct can undergo a desired physical transformation can be fine-tuned and modulated by varying the functional chemistry of the biomaterial, as well as the ratio of the various chemical substituents of the bioink formulation. It should be noted, however, that not all trigger sources for 4D transformations are appropriate for bioprinted constructs, as will be discussed further in the 'Bioprinting' section.

In the present review, a general overview of the cortical tissues of the brain and a few crucial developmental aspects of cortical folding are reviewed. Herein, the two major contemporary models of cortical folding are analyzed by overviewing the computational, materials, and cell-based studies which have developed them. 4D bioprinting as a viable methodology for fabricating 'smart', living tissue constructs by which to analyze the nuances of cortical folding biomechanics, and the effects these forces have on further neuro-development are then introduced. Our discussion of 4D bioprinting of neural tissues includes a general outline of current 3D- and 4D-printing technologies. We conclude our discussion with a brief overview of recent advancements in 3D- and 4D bioprinting of nervous system tissues, and discuss plausible directions future research might take towards a robust 4D-bioprinted platform for studying the motile aspects of neurodevelopment and disease.

2. The neurobiology of cortical folding

Due to the complex and highly interconnected nature of the brain's tissues, its physiology and development are exceedingly difficult to model both computationally and *in vitro* [45]. Arguably, one of the most challenging facets of neurodevelopment to simulate is the mechanical folding of the cortical tissues. Namely, there are two cortical regions of the brain; the cortex of the cerebrum, known as the cerebral cortex, and the cortex of the cerebellum, known as the cerebellar cortex. The process of cortical folding of the cerebral cortex is known as 'gyrification', whereas the analogous process of cortical folding in the cerebellum is known simply as 'foliation'. The actual processes which guide the folding patterns of these two cortical tissues are different in some respects, but share many biomechanical similarities. In order to better discuss the processes of the cortical folding across the cerebrum and the cerebellum, it is useful to first consider a few key aspects of the brain's gross anatomy as well as fundamental cytoarchitectural elements involved in neurodevelopment.

2.1. Overview of gross brain anatomy

The brain is anatomically partitioned into four interconnected tissue subsystems and is composed of an estimated 86 billion neurons, and some 85 billion non-neuronal cells [46,47]. In brief, the general tissue subsystems of the brain include the cerebrum (which is divided into two cerebral hemispheres), the brainstem, the diencephalon, and the cerebellum [46]. The brainstem is comprised of 3 main parts: (i) the midbrain

(mesencephalon), which is associated with motor functioning; (ii) the pons, which encompasses several cranial nerve nuclei and serves as an important conduit for bidirectional neural tracts; and (iii) the medulla, which largely functions to regulate vital processes such as heart contraction and breathing [46,48]. The cerebellum or 'little-brain' is located adjacent to the brainstem in the posterior cranial fossa. Its distinctive exterior is composed of many fine grooves of undulating tissue known as folia, and as a whole, is largely associated with motor control and muscle memory [46,48]. The forebrain is composed of both the cerebrum and the diencephalon. The diencephalon houses both the thalamus, which serves as a cortical relay, and the hypothalamus, which largely works to modulate autonomic functions such as the regulation of body temperature [46,48]. The cerebrum is the largest portion of the brain and is divided into two, non-symmetrical hemispheres which entail the cerebral cortex, basal ganglia, hippocampus, and amygdala [46,48–50].

2.2. Cortical tissues of the cerebrum and the cerebellum

The cerebral hemispheres (as well as the cerebellum), are comprised of two distinct types of tissue matter: (i) a stratified gray matter which forms the outermost cortical layers; and (ii) the underlying white matter which is composed of myelinated projection, association, and commissural fibers which work to connect the different cortical regions to one another and to the other subsystems of the brain [46,50,51]. In both the cerebrum and cerebellum, the connecting fibers of white matter help to undergird the convoluting ridges of cortical tissue, known as gyri in the former and folia in the latter. The fissures of varying depth which lie between adjacent gyri and folia are known as sulci [46,52]. These ridges and fissures effectively work to increase the brain's surface area which allows for higher densities of neurons and supporting glia to occupy the cortical layers than what would be possible if the cortex was smooth (lissencephalic) instead. The convoluted topology of the cerebral cortex serves in part to divide the cerebral hemispheres into four discrete primary lateral regions, known as the frontal, parietal, temporal, and occipital lobes [46,50]. The cortical tissue which comprises each lobe is further divided into some 52 smaller Brodmann areas, which are highly interconnected and house unique networks of neural circuitry [46]. Each Brodmann area is believed to be associated with the regulation of a unique set of cognitive, sensory processing, and behavioral functions [46,53]. By extension, it is very likely that proper gyrification is imperative for the successful establishment, organization, and functioning of the unique neural circuitry that innervates each discrete Brodmann area, as well as the white matter projections which interconnect them. Thereby, it can likely be postulated that aberrant cortical folding in the cerebrum negatively impacts cognition by disrupting the autonomic functioning and interconnectivity of the Brodmann areas on an individual to a regional basis.

In a similar manner to the cerebral cortex, the cortex of the cerebellum is itself divided into many physiologically functioning, anatomical units known as longitudinal 'micro-zones' which are constituted by the principal cortical neurons themselves [54]. Expanding upon the micro-zone-based functional unit model which was originally proposed by Oscarsson, the work of Masao Ito has suggested that the complete

cerebellar functional unit includes not only the neurons of the cortical circuit, but also includes the subcortical nuclei as well, in what has been deemed as a cerebellar 'micro-complex' [55]. The cerebellar cortex is estimated to house some 5000 of these micro-complexes, whereby each region of the cortical circuit is connected throughout the cortex to the brain stem, and/or spinal cord through projections to and from the cerebellar and vestibular nuclei, inferior olive, and the parvicellular red nucleus [56]. It is believed that each micro-complex receives sensory-motor information originating from elsewhere in the brain as well as the peripheral nervous system (PNS), and is in turn responsible for actuating unique modulatory controls directly corresponding to specific motor regions of the body.

The tissues of both the cerebral and cerebellar cortex are highly stratified and are composed of a diverse array of neural and glial cell types which arrange in complex, hierarchal patterns. The establishment of these hierarchal patterns arises during early neurodevelopment and are inter-related with the folding of their resident tissues. The cortex of the cerebrum has a typical thickness of approximately 2.5 mm, and stratifies into six discrete layers (I-VI) which contain a range of glial cell-types as well as an abundance of pyramidal and Betz neurons [57]. The cerebellar cortex on the other hand typically has a thickness of around 1.2 mm and stratifies into three layers; namely the granular, Purkinje, and molecular layers [58]. The major input of the cerebellar cortex arises through excitatory climbing and mossy fibers, while the sole output of the cerebellar circuit is inhibitory by means of GABAergic synapses of the Purkinje neurons onto the deep cerebellar nuclei (DCN) [55,56]. The cerebellar cortex contains a massively parallel network of axonal processes of granular cells, which are by far the most populous neural cell-type in the entire body.

Evidence suggests that the organization of the neural cells which are observed in both types of maturing cortical tissues rely heavily on the migration of neural progenitor cells across the cellular processes of specialized glia cells known as radial glial cells (RGCs) [59]. As neural progenitor and stem cells migrate, they begin to differentiate, and thus extend axonal projections of their own. These early axonal projections begin to interconnect various regions of the developing cortex, as well as connect with the subcortical white matter. The stresses created by early axonal connectivity as well as the manner and rate in which early progenitor and neural stem cells proliferate within regions of the developing cortex form the practical basis of the two primary models of cortical folding which will be discussed herein.

3. Current models of cortical folding

3.1. Axonal tension model of cortical folding

The core hypothesis of the axonal tension model of cortical folding, originally proposed by Van Essen, posits that radial anisotropy and connectivity of neuronal axonal processes to one another and to white matter resident nuclei lead to differential local tensions and tensions at length [7]. This hypothesis supposes that differences in tension, in turn, cause some areas of the cortex to be pulled closer together, which can lead to inward or outward oriented surface buckling, as is shown in Figure 1.

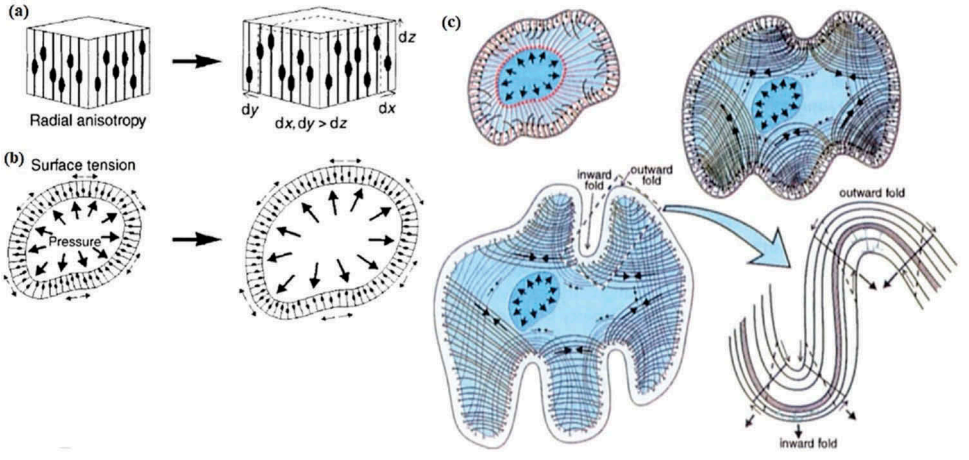

Figure 1. Anisotropic growth mechanisms of tissue expansion and tension model of cortical folding. (a) Diagram of a neuroepithelial sheet which depicts preferential tangential expansion over radial expansion. This hypothetical anisotropic model supposes that radial rigidity, which arises from cellular processes being under tension, constrains vertical growth. (b) A proposed swelling balloon-like model neuroepithelium which sees tangential expansion further arising from outward pressure exerted from ventricular fluid and compressive surface tensions about the radial axis. (c) Neural cells (small black circles) migrate along radial glia (red circles with line-like processes) and begin to extend axonal processes. The hypothetical model proposes that as these processes reach localized targets, adjacent regions become more connected, while more remote regions drift further apart (less connected). Local tensions are hypothesized to become stronger than tensions at length between distant regions, and thus would theoretically promote tangential expansion mediated folding. Adapted with permission from [7].

This hypothetical model of folding posits that initially the thin cortical layers are tethered to the underlying white matter through the processes of RGCs. As neural cells migrate along the axis of RGCs, they extend axonal processes of differing lengths toward circuit-specific cellular targets (and towards subcortical structures) Figure 1c. The central hypothesis of this model supposes that the differences in length of the axonal projections, their directionality, the number of connections formed, and the visco-elastic properties of the neurites themselves provide sufficient tensile forces necessary to induce cortical buckling [7]. This model postulates that these neurite projections form before cortical folding is observed, and as more connections arise, greater tension begins to develop between linked portions of tissue. In this model, folding would be non-random, as the primary-most driving force behind cortical plate buckling would be the establishment of specific axonal connections. To this end, the ability of axonal projections to find and form strong synaptic connections upon their targets is imperative [7]. By extension, the distance which axonal processes would need to be extended to reach their targets would hypothetically have a considerable net effect on the tensile force each axon could exert, and on their rigidity. Shorter axonal connections would likely exert greater force over a smaller area and would thus be more rigid than longer axonal projections. However, as argued by other sources, discerning whether or not the presence and morphology of local short axonal connections is a cause of cortical folding or is rather a function of stability and conservation of energy, is difficult [16,60]. Whereas

there is some evidence which suggests that axonal tension may play some role in the formation of cortical folds, the microdissection work of Xu et al. (2010) has demonstrated that axonal tension is not directed across areas undergoing gyration, challenging the speculation that axonal tension is the key driving force of cortical folding [61].

3.2. Tangential expansion model of cortical folding

In the differential tangential expansion model of cortical folding, surface instabilities give rise to predictable folding patterns. Put simply, this description of the cortical folding mechanism posits that differential tangential growth of regions of the cortex exerts expansive pressures on the localized tissue. Therein, this tangential expansion causes cortical buckling which in turn manifests in the formation of discrete gyri/folia and sulci [10].

From a strictly mechanical perspective, the surface-folding profile of any bi-laminar system is contingent on two intrinsic aspects of the material system; (i) the thickness of the respective layers and (ii) the effective modulus (stiffness) of each layer. As a general trend, the thicker the bottom layer is, the more constrained tangential expansion becomes in the upper layer, which in turn will decrease both the folding wavelength and fold amplitude. A similar decrease in both folding wavelength and fold amplitude would be seen if the modulus of the lower layer is sufficiently greater than that of the top layer.

An early model of cortical folding proposed by Richman *et al.* suggested that the white matter of the brain was highly elastic and that the gray-matter could be simulated by two laminar sheets which were bound to the elastic underlayment, and to one another. Richman's model generally predicts that if the superficial-most layer of the system expands at a greater rate than the deeper layer, then stress will be generated, which will cause predictable surface buckling to occur according to the expression:

$$f(x,y) = \sin\left(\frac{2\pi x}{l_x}\right)\sin\left(\frac{2\pi y}{l_y}\right) \tag{1}$$

Wherein l_x and l_y represent the wavelength of layer-buckling in the x and y coordinates, respectively [62].

With this prediction, differential growth of the superficial layer of cortical tissue, in turn, yields a multitude of possible sinusoidal folding patterns, which appear to be in relative agreement with *in vivo* cortical folding trends [62]. It is worth noting, as is mentioned elsewhere, that this early predictive model does not consider that the white matter of the brain has a similar modulus/elasticity to the gray-matter [10,16,61]. In a practical sense, this model has notable application in predicting the general scheme in which cortical folds will form, but does not account for the underlying source of the differential growth which drives tangential expansion. Namely, this model would be effective in predicting how spread apart folds will occur, but cannot, in reality, be used to predict the exact physiological location in the real cortical tissue where folding will initiate.

A recent study used a combined computational and materials-based approach to study the effects that differential tangential expansion within the upper layer of a bi-laminar system has on the generation of surface instability. Therein, resultant surface instability

functions as the primary driver of the cortical folding [17]. In this study, researchers used the common elastomer polydimethylsiloxane (PDMS) to generate a bi-layered model of brain tissue which could be modified to exhibit variable upper and lower layer stiffnesses in an effort to recreate surface folding, as depicted in Figure 2. In this model, the upper PDMS layer represented the gray matter of the brain, while the thicker lower layer represented the white matter. The study design involved varying the stiffnesses of the layers in three discrete schemes; (i) {stiff upper layer/soft lower layer}, (ii) {soft upper layer/stiff lower layer}, and (iii) {soft upper layer/soft lower layer} Figure 2 (a)–(f). Therein, each bi-layer model was submerged into a solution of hexane in order to induce surface swelling (expansion) in order to study the resulting folding patterns Figure 2 (g). It was ultimately found that if the two elastomer layers possessed similar moduli, then the surface expansion yielded folding patterns most similar to the gyri and sulci of the cerebral cortex, as shown by Figure 2 (c).

This elastomeric model of cortical folding was further expanded by the same research group (Tallinen *et al.* 2016) wherein magnetic resonance images (MRI) of 22-week-old human fetal brains were taken and were used to create a 3D printed brain mold [18]. At around 22 weeks of gestation, the human brain is relatively smooth, wherein it begins to form its stereotyped wrinkled topology around week 23. Researchers made a silicone-based negative cast from the printed structure and used this silicon cast to create an elastomeric core to simulate the white matter of the brain, as shown in Figure 3 (a). The core structure was then coated in swellable polymer to simulate the gray matter. The construct was then subjected to solvent immersion which caused the outer-most

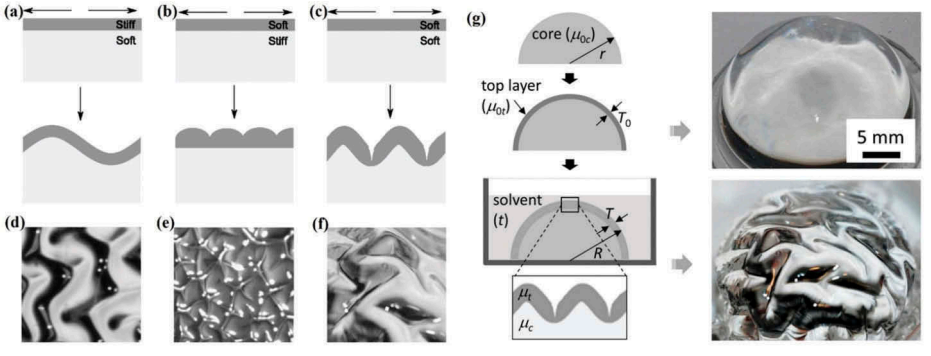

Figure 2. Surface swellability leads to different cortical folding patterns. (a) Sinusoidal folding occurs when the upper layer (gray matter) is stiffer than the lower layer (white matter) of a growing bi-layer cortical model. (b) Cupsed folding occurs when the upper layer is softer than the lower layer. (c) Distinctive gyri and sulci arise when both the upper and lower layers have similar stiffnesses. (d-f) show the folding patterns of bi-layer gels which arise from differential swelling. The resultant patterns demonstrate the sinusoidal, cupsed, and gyri/sulci folding predicted by (a)-(c) respectively. (g) Elastomer model of the brain folding constructed by making a core hemisphere of radius (r) which has a shear modulus of (μ_{0c}). The hemispheric core is coated in a thin layer of polymer with a thickness (T_0) which exhibits a shear modulus of (μ_{0t}). The top and core (or upper and lower) layers have a combined radius (R). The completed model is then submeregd in solvent and allowed to swell for time (t). When the moduli of both the top and core layers are similar (moduli ratio $\mu_t/\mu_c \approx 1$) the distinct gyri/sulci folding pattern from (c) arises. Adapted with permission from [17].

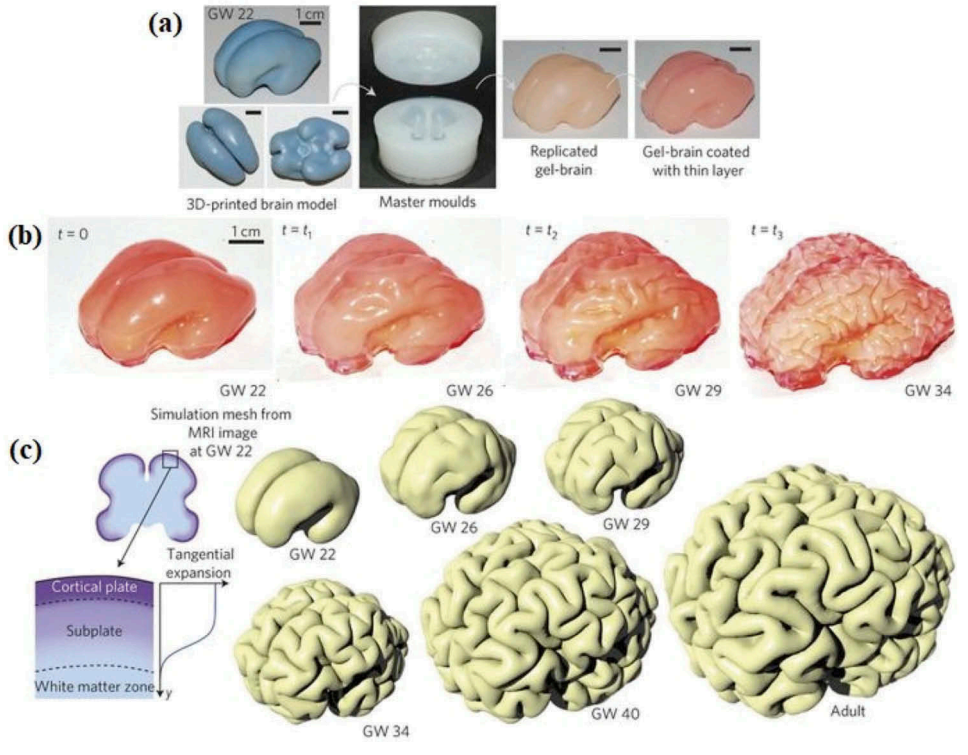

Figure 3. Cortical expansion simulated by a swellable brain model and comparison to computer simulation of the folding pattern of the *in vivo* brain. (a) 3D printed model of the smooth human brain at gestational week 22. The 3D printed smooth brain was used to make a silicone mold, which served as a cast for the gel-brain model. The gel model was then coated with a thin, swellable layer. (b) Folding patterns arising from differential swelling of the outer layer of the gel-brain model at times $t_0 = 0$ mins, $t_1 = 4$ mins, $t_2 = 9$ mins, $t_3 = 16$ mins post-submersion in a hexane solution. (c) Computer simulation of cortical folding which arises from tangential expansion at gestational weeks 22, 26, 29, 34, and 40, and yields the stereotyped wrinkled patterns observed by adulthood. The model folding patterns at times t_0-t_3 in (b) highly resemble the simulated cortical wrinkling at gestational weeks 22, 26, 29, and 34 respectively in (c). Adapted with permission from [18].

elastomer to expand and generate buckles in a manner which highly resembles *in vivo* cortical folding [18] Figure 3 (b-c).

The study does well to demonstrate that initial folding is largely a function of cortical swelling induced instabilities which confers stereotyped buckling. As with the other elastomer-based model, this study aims to elucidate the mechanism of cortical folding alone, and largely does not take into consideration the effects mechanical folding forces, such as stretching, compression, and stiffening, have on further neural-cell organization and commitment [63–66]. This model of cortical folding also sees the folding process occur at a rate which is far faster than what is observed *in vivo*. Namely, the speeds at which the buckling and subsequent folding occur, may in fact play a role in determining the depth of buckling and the specific geometries of the sulci which form. The folds of the brain take weeks to form, while this experiment showed brain-like folding which occurred within minutes.

The models of cortical folding which we have so far discussed have primarily focused on computational and cell-devoid materials-based approaches to study the underlying mechanical processes of folding. However, in actuality, there are likely several different mechanical processes which coalesce to guide the folding phenomenon. From a materials and computational modeling standpoint, it is important to analyze the degree to which internal stresses can predict the morphology of cortical folds in both standard and perturbed conditions and compare the results to what is observed *in vivo*. Thereby, to truly test the validity of these models, their predictions should be recapitulated by *in vitro* cell models of cortical folding. As such, a recent study used a brain-organoid-on-a-chip to study the biophysical mechanisms which underlie cortical folding in the context of living cells [25]. In this unique study, human embryonic stem cells hESCs were grown within a Matrigel^{TM} matrix in order to form millimeter scale brain organoids, as is described in Figure 4. Researchers observed distinct radial nuclear orientation, and by day 30 of the study, immunostaining revealed that the organoids accurately depicted early neural development. The chip construct design held the organoids in a media reservoir, compressing them between a coverslip and a membrane, shown by Figure 4 (a). This method of compressing and submerging the organoids in media may have played a critical role in dissuading the organoid core cell death that typically plagues organoid studies at the millimeter scale. This compression might have also imparted additional mechanical stresses on the cells within the organoid which could have in turn biased their folding patterns. On the other hand, this compression may have also helped to simulate the extrinsic physical constraint that the skull imparts on the expanding cortex. Surface instabilities arose at days 6–11 Figure 4 (c), and it was found that a nuclear density of $\rho_c = 0.85 \pm 0.1$ sees an increase in wrinkling transition Figure 4(g). The wrinkling wavelength λ, the distance between gyri, was also found to have a positive linear relationship with outer layer thickness. The surface folding of the organoid study was also compared to MRI images of fetal brains, which showed that the organoids folded in a similar manner to *in vivo* cortical tissues. While these folding trends were consistent, the authors suggest that their organoids mostly consisted of neural progenitors, while fetal cortical tissue mostly consists of maturing radial neurons. The authors conclude that their study demonstrates that for organoids studies, surface layer folding is likely a function of increased growth coupled with cell contraction within the organoid core. Although there are some notable dissimilarities between the cellular mechanisms of organoid and *in vivo* cortical tissue folding, the findings of this study are seemingly consistent with the differential tangential expansion explanation proposed by the computational and materials-based models that have been presented.

Taken together, the computational, materials-based, and organoid studies that have been conducted in order to study the biophysical mechanisms which guide the cortical folding of the brain have indeed provided crucial insights into how the process likely occurs *in vivo*. However, to gain a more comprehensive description of how the processes are initiated in the cortical tissues, and to further study the manner in which folding associated mechanical stresses impact neurodevelopment from a cell biology perspective, additive tissue engineering approaches are likely necessary. In particular, a strong case for using both 3D and 4D-bioprinting methodologies towards this aim can be made [44, 67,68].

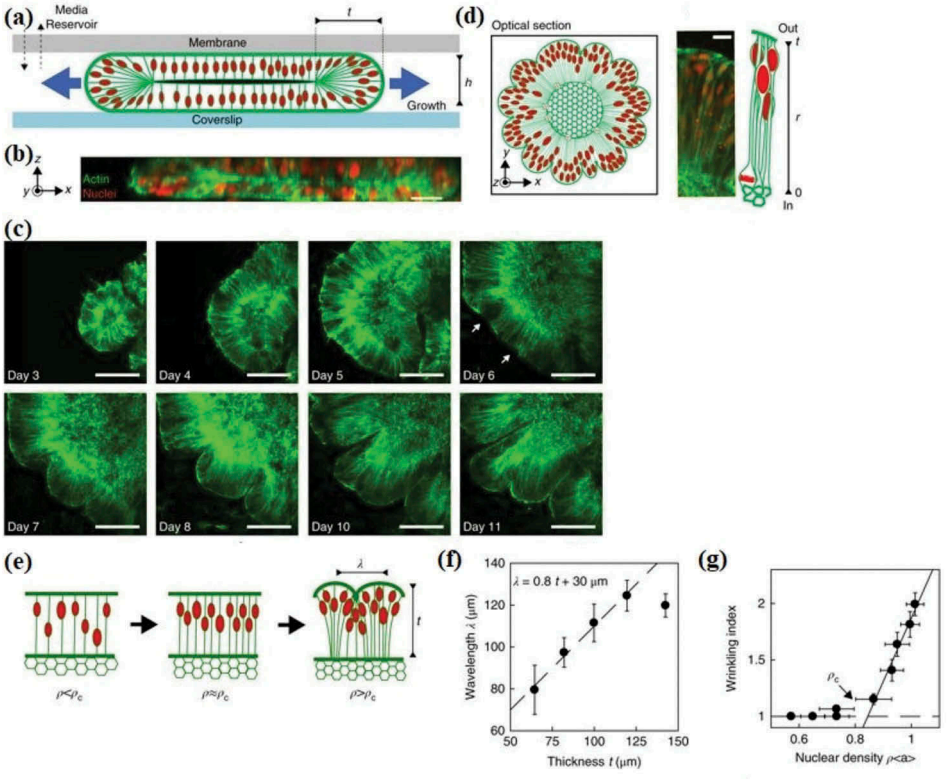

Figure 4. Brain organoid-on-a-chip model of cortical folding. (a) Schematic of neural organoid-on -a-chip system where the organoid is compressed between a coverslip and a media permeable membrane. (t) represents the organoid's thickness while (h) represents the distance between the coverslip and the membrane, which is equal to 150μm. (b) Side-view (Z-stack) of organoid with Lifeact-GFP stained actin (green) and H2B-mCherry stained nuclei (red). (c) Development of organoid wrinkling from days 3–11 (arrows denote initial surface instability which yielded further formation of wrinkles). (d) Top-down view of neural organoid showing bi-polar morphology and nuclear distribution. Organoid has an inner surface (r= 0) and an outer surface (r= t). (e) Outer layer wrinkling arises as the nuclear density (ρ) exceeds a critical density threshold (ρ_c), $\rho > \rho_c$. (f) Linear relationship between thickness (t) and wrinkle wavelength (λ). (g) Relationship between nuclear density $\rho <$ a> and Wrinkling index. A critical nuclear density $\rho_c = 0.85 \pm 0.1 <$ a> shows a notable increase in wrinkle formation. Adapted with permission from [25].

4. 4D bioprinting

The concept of 4D-printing was first introduced by Skylar Tibbits and his MIT team, as is described in their 2014 publication [69]. As mentioned previously, 4D-printed objects are essentially defined as being 3D printed objects which as a function of some intrinsic component of their design and composition, display certain attributes that are temporally variable. Although there are several physical characteristics which can be transformed over time within a 4D-bioprinted construct, most 4D objects changes in shape and spatial organization. There is some debate in the field of additive manufacturing as to what qualifies as a 4D attribute with respect to a printed construct, but as a general

trend, degradation and color changes are not typically regarded as being truly 4D, as they are seen as being overly difficult to control. In the case of degradation, an argument has been made that the printed object itself has to participate in or be a 'carrier' of the physical transformation, rather than simply disappear itself as a function of time [36].

Both 3D and 4D printing rely on the utilization of both printing platforms and appropriate printing materials, whether they are thermoplastics, ceramics, hydrogels, or polymers [44,68]. In the case of bioprinting, fabricated constructs can be printed devoid of cells initially and can be later seeded (scaffold-based) or the constructs themselves can be cell-bearing, wherein the printing material (bioink) encapsulates living cells which are printed into complex, predesigned patterns. In both 3D and 4D bioprinting, the printing process must itself not be harmful to encapsulated cells. Specifically in the case of 4D bioprinting, the physical manner in which the printed construct changes in response to the exogenous trigger, as well as the triggering mechanism itself must also be mild on both seeded and encapsulated cells. As mentioned previously, there have been a multitude of triggering mechanisms which have been explored to induce transformations within 4D-printed constructs, though many are harmful to resident cells.

Possibly the most practical means for a 4D construct to be triggered into transforming its shape is through the differential, localized swellability within the material. A major factor in consideration for using this methodology for triggering a 4D transformation in the form of shape change is the cytotoxicity of the solvent that the material is subjected to. Ideally, a solvent such as growth media, PBS, or even water would be the most favorable for cell-laden constructs. Interestingly, a recent study found that a hydrogel ink with aligned cellulose fibrils could be printed into highly biomimetic flower-like architectures and could be made to curl and twist when subjected to water immersion at varying temperatures [37]. Moreover, it was found that the addition of poly (N-isopropylacrylamide) to the ink formulation allowed for the shape changes to become reversible. The results of this study demonstrated that folding geometry could be tuned and modified by varying print infill density and localized anisotropy, combined with the alignment of microfeatures within the ink formulation. As a result of the experimental ink's high potential to enact controlled stretching and folding across the construct in response to water submersion, a similar ink could potentially make an excellent candidate for fabricating a cortical folding model.

4.1. Considerations for 4D-bioprinting neural tissues constructs

In the endeavor to model the processes of cortical tissue folding with a 4D-bioprinting approach, there are several pivotal developmental and tissue-specific aspects which should be considered in the construct design process. In this way, a cell-based model of the developing cortical tissues of the brain should be sufficiently biomimetic and should undergo the folding process in a physiologically relevant manner. Specifically, for a bioprinted tissue construct to be biomimetic, the modulus of the printed tissue networks should be similar to that of the *in vivo* gray and white matter. Namely, a 4D-printed brain tissue construct should be made to have a cerebral gray matter modulus of 0.68 ± 0.20 kPa, a cerebral white matter modulus of 1.41 ± 0.66 kPa, and moduli of

0.75 ± 0.29 kPa for both the gray and white matters of the cerebellum [12]. In the case of printable hydrogels, which may be the most effective type of material to fabricate complex neural tissue constructs, the material modulus can be readily altered by varying crosslinker concentration or crosslinking conditions. It has been found that the modulus of a hydrogel has a substantial effect on the proliferation and differentiation of neural stem cells [70]. Therein, it was observed that increasing the modulus of a hydrogel had a negative impact on both NSC proliferation rate as well as the expression of the neural differentiation marker β-tubulin III. In the case of a folding soft material such as a hydrogel, the areas at the crests and troughs of the forming folds observe a substantial localized change in material modulus. This change in the localized effective modulus around the pivot points of the 4D-printed construct can likely be modulated through the incorporation of multiple printing inks with different mechanical properties. Therein, the addition of multiple printing materials with varying stiffnesses or thicknesses can be used to predetermine folding patterns in order to mimic the various folding regimes of the brain's cortical regions. For example, a tandem stereolithography/bioplotting approach can be used to fabricate a multi-material system with thick lower layers and thin upper layers in order to accurately replicate the short wavelength and shallow amplitude folds of the cerebellum.

As it has been demonstrated previously, mechanical forces and mechanosensing play a crucial role in neural-cell fate-assumption and organization, it would be logical to hypothesize that in the case of a foldable, 4D-printed hydrogel system with encapsulated NSCs, one would expect to see notable differentiation and cell migration around the peaks and valleys of the forming folds [63–66]. However, at the current state of 4D printing of smart materials, it is difficult to precisely control the exact time and force with which a printed construct can fold. Thereby, it would be difficult to control and quantify the stresses which encapsulated cells experience around the folding crests and troughs. Therefore, future cell-based models of cortical folding should include cell viabilities assays to ensure that the cell populations and proliferation rates around the pivot points are in fact representative of *in vivo* cortical folds.

Another critical point to consider in designing a 4D-bioprinted model of cortical folding is the rate at which the 4D construct enfolds, as mentioned previously. In order to be sufficiently biomimetic, a 4D-bioprinted cortical model should be made to gyrate or foliate over the course of 10 or more weeks *in vitro*. Therein, 4D capable thermoset SMPs might be a favorable class of biomaterial to explore, owing to their ease of modification and their generalized sensitivity to thermo-induced shape changes across a range of temperatures. In general, thermosensitive SMPs often take the form of thermoset polymeric compounds which are blended into thermo-curable resins. These resins are often heated to produce irreversible crosslinking across polymeric substituents as the construct is fabricated/shaped into an original conformation. In addition to thermo-curing SMPs into permanent shapes, they can also be photocured with UV light [34–36]. The unique feature of these thermo-responsive polymers is that they have a specific temperature at which they become increasingly more pliable, known as the transition temperature T_{trans}, wherein if the temperature of the printed SMP is heated past this critical temperature $T_{construct} \geq T_{trans}$ the construct can be easily molded into a temporary shape. Once the temperature of the SMP construct falls below the transition temperature, $T_{construct} < T_{trans}$, the polymer re-hardens, and as a result, the

construct becomes affixed in its temporary shape. When the temperature of the SMP again re-approaches the transitional temperature, the construct will begin to re-assume its original, permanent shape and conformation.

Recently, our group formulated an experimental array of novel biocompatible SMP formulations to explore their potential utility for 4D-bioprinting and tissue regenerative applications [33–35,44]. It was found that the various polymeric formulations could be affixed at −18°C into temporary conformations which folded back upon themselves at an angle of 180°, and could fully recover their original shape at 37°C. Whereas the slowest speed of recovery (3.9°/s recovery, material C20P300PH) was still substantially faster than what would be required to make a truly biomimetic model of cortical folding, the results remain encouraging because they illustrate the wide range of shape transformation speeds that are possible with various SMPs. If the material which yielded the slowest recovery time (C20P300PH) could be chemically modified so that its glass transition temperature T_{gc} could be increased above 35°C, then its recovery time could possibly be slowed down to a multiple week time-scale.

In a similar manner to how the SMPs of our above-mentioned study could reassume their original shape at a physiologically relevant temperature, constructs fabricated from a novel soybean oil epoxidized acrylate (SOEA) bioink could also recover their printed shape at 37°C, as outlined in Figure 5. Using a photolithographic-stereolithographic-tandem fabrication technique the SEOA was fabricated into a heart shape which displayed a rolled or curled post-printing original shape. Specifically, the heart shape was partially photocrosslinked using a mask cut-out, and was then further functionalized with micropatterned grooves using a stereolithography printing system, Figure 5(a). Once printed, the heart construct was able to be affixed into a flat temporary shape, and was able to recover its original rolled shape at 37°C, Figure 5 (b-c). As with the SMPs formulated in the previously mentioned study, the SOEA-based 4D construct recovered its original shape at a timescale that was far faster than what could be used to simulate cortical folding. However, the composition of the SOEA ink may be tuned and modified to promote a slower shape-recovery regime at physiological temperatures.

In addition to the ability of the printing material to change its shape in a physiologically relevant manner, a 4D-bioprinted construct should also contain brain and general neural tissue compatible growth factors and biomolecular components, such as hyaluronic acid (HA) and lectins. Fortunately, many of the hydrogels, SMPs, and biodegradable elastomers [71] that have been explored for use in 4D-bioprinting and biomedical applications have readily modifiable surface chemistries, which can be appended with bioactive components. In the case of 4D enabled hydrogels, many pertinent brain-associated ECM components can be readily mixed into the ink formulation without the need of chemical modification due to their hydrophilicity.

4.2. Bioprinting technologies

Whereas there are a variety of bioprinting technologies that have been developed, not all printing approaches are necessarily appropriate for the fabrication of complex brain tissues. However, due to the ever-expanding research in materials science, 3D/4D printing, and tissue engineering approaches, what might not seem useful for these kinds of studies currently, may, in turn, yield promising results through the technological

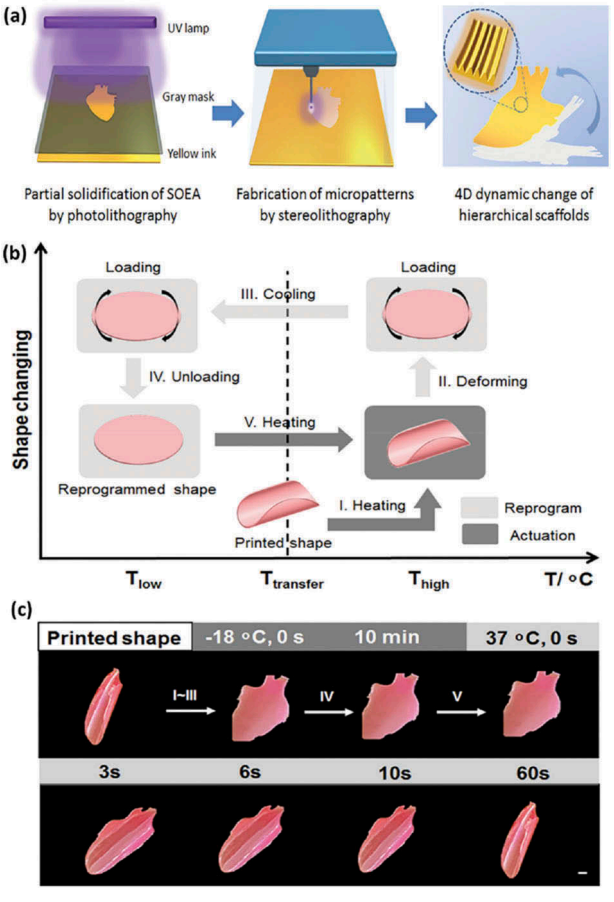

Figure 5. A 4D printed thermally sensitive natural soybean oil epoxidized acrylate (SOEA) constructs developed in our lab. (a) A tandem photolithography-stereolithography process to fabricate heart-shaped constructs from novel soybean oil epoxidized acrylate. (b) Schematic illustration of the 4D shape memory process triggered by temperature. (c) Rolled heart-shaped SOEA constructs can be affixed into flat temporary shapes at −18°C and can fully recover their original shape at 37°C. Scale bar, 2 mm. Adapted with permission from [35].

advancements of the near future [72]. As such, the following section includes an overview of many types of printing technologies, which are useful for fabricating neurological, as well as other complex tissue constructs.

4.2.1. Inkjet bioprinting

Inkjet bioprinting or drop-on-demand printing is a printing methodology which often uses modified commercial grade inkjet printers to deposit living cells (or biomolecules such as proteins or growth factors [73]) in a dropwise manner [74]. In this bioprinting technique, cells and other biomaterials are suspended in a liquid solution known as a 'bioink' and are ejected from a print nozzle onto a desired surface (often a refined glass sheet or a silicon wafer, known as a 'biopaper'), to build a drop-by-drop structure from a predesigned pattern. Inkjet printing, like most other bioprinting technologies, utilizes

computer-aided design (CAD) renderings to guide the droplet deposition to form the desired construct shape and form. The resolution at which a construct can be produced with inkjet printing can be controlled by varying the droplet volume (<1pL to >300pL), the encapsulated cell concentration (1–2 cells per drop, with overall bulk cell concentrations of <106 cells/ml), and the print rate (1–10,000 droplets per second) [75]. Inkjet bioprinters can dispense bioink droplets by either cycling the local temperature within the printing apparatus through resistive heating elements (thermal inkjets) [76] or through piezoelectric pulses through an actuator [75]. One consideration that must be made when using any bioprinting technology is the potential detrimental effects that the printing apparatus might impact on the survivability of the cells encapsulated in the bioink during the printing process. Studies have found that despite the considerable heat that encapsulated cells are subjected to in inkjet bioprinters (≤300°C), there is negligible impact on printed cell integrity, allowing for >89% post-printing viability [77,78]. This observation is possibly explained in part by the considerably brief amount of time individual cells in the ink flow spend in close proximity to the heating elements. An additional advantage to inkjet bioprinting is that it can print multiple cell types simultaneously [79]. However, a critical limitation of inkjet bioprinting is that the printing apparatus is prone to clogging at the print nozzle, and thus requires bioink formulations to assume relatively low viscosities in the range of 3.5–12 mPa/s [75]. The issue therein is that in order for a printed construct to mimic the microarchitecture of *in vivo* tissues, it must maintain high shape fidelity to the original design post-printing. As such, lowering the viscosity of the bioink decreases its capacity to hold its shape upon deposition on the biopaper. Therefore, inkjet bioprinters are able to print constructs with high cellular and biomolecular resolution, but with mid-to-lower shape fidelity. Since there is currently a limited amount of 4D capable hydrogels, 4D inkjet bioprinting is still in its infancy.

4.2.2. Extrusion-based bioprinting

Extrusion-based bioprinting methodologies are by far the best characterized and widely utilized means of fabricating complex biomaterial constructs. Extrusion bioprinting technologies, including direct-ink-writing micro-extrusion printing, bioplotting, and fused deposition modeling (FDM), utilize a controlled ejection of continuous streams (or spheroids) of bioinks and thermoplastics onto a flat print surface in a layer-by-layer manner to fabricate tissue constructs [74,75]. These technologies can be used to generate cell-laden (or cell-devoid) hydrogels [80,81] or layered scaffolds of interconnected thermo-ink networks by which cells can be seeded [82]. FDM involves the drawing of a thermoplastic material, such as polycaprolactone (PCL), through a heating element in order to be liquified and subsequently extruded through a nozzle into layered filaments. Due to the initial solid form of the printable material, and the considerable temperature that the material must be heated to (≥120°C) in order to melt [82,83], traditional FDM approaches do not readily allow for the printing of live (encapsulated) cells [83]. As such, FDM is largely used to print porous networks of layered filaments that are manually seeded with cells. Whereas one study showed that PCL can be printed into a construct with considerable uniformity (at 61% porosity) and subsequently seeded with fibroblasts [82], there is some skepticism as to whether standard FDM techniques can be used to print more complex tissue geometries,

such as those of the brain, with appropriate accuracy (as general FDM printers have been found to show a wide print accuracy range of ± 127μm) [84].

Bioplotting and micro-extrusion printing, in contrast to FDM, can be used to print a wide variety of cell-laden (and non-cellular) bioinks including ink materials that have been shown to promote cell viability and proliferation, such as alginate [85], gelatin [81,85], GelMA/PEGTA [80], modified Gellan Gum [28], Fibrin/Collagen [29], and multi-combinatorial alginate/chitosan/agarose [30,86] bioinks. Bioplotting and micro-extrusion printing can be used to print both individual and mixed cell cultures and show greater promise in fabricating constructs that display considerable mimicry of the cytological heterogeneity of *in vivo* tissues.

Both 4D Direct ink writing (DIW) and FDM involve the assemblage of layer-by-layer 3D constructs that are subjected to shape-change initiation post-printing. Of the two forms of extrusion printing, DIW is likely the most suitable candidate for 4D-bioprinting applications as DIW inks are often soft materials such as hydrogels, which effectively mimic the ECM and effective modulus of many native tissues. The majority of the 4D shape effects that bioplotted or direct ink written constructs are capable of are contingent on the printed materials' swellability, the alignment of microscale components within the ink, and localized anisotropy of printed features [36,37].

4.2.3. Selective laser sintering

Selective laser sintering is an additive manufacturing technique originally developed in the mid-1980s, whereby a long wavelength laser (or other high energy electromagnetic radiation source) is directed upon a reservoir of powdered or beaded solid material to induced localized melting and fusion of the solid material in a layer-by-layer manner, forming a 3D pattern as new layers of additional sintering material are filled in [74,87]. To date, common sintering materials have included Nylon [88], PCL [89], and hydroxyapatite composites with polyvinyl alcohol [90], PLGA/hydroxyapatite, and PCL/hydroxyapatite [87,91]. In quite the similar manner as FDM printing, SLS cannot foreseeably be used to directly bioprint encapsulated cells into the forming construct due to both the solid nature of the print material as well as the preclusive high local temperatures requisite for the polymer material to melt. An additional limitation of SLS utilization for bioprinting is depreciated fidelity of the printed construct to the original shape design caused by the spreading of the melting polymer away from the focal point of the directed laser and subsequent further degradation of the polymer. As such, a modified approach to SLS known as Surface SLS was developed whereby selective heating of carbon coated poly(D, L-lactic) acid (PLA) to help compensate for the polymer degradation problem, but was only able to yield a spatial resolution of ~100-200μm [88], which is likely too large for the fabrication of more complex tissue types. Additionally, SLS (much like FDM) yields considerably rigid scaffold networks which are likely unfavorable for soft neural tissues. These rigid scaffolds also likely require a high level of fibroblast cell seeding before other cell types could effectively adhere, in contrast to the ECM mimicry of hydrogels which can be made from dECMs.

4.2.4. Laser-assisted printing (laser-induced forward transfer)

Laser-induced forward transfer (LIFT) printing is a unique technique to print cells or other biomolecules onto a substrate in a designated pattern. The LIFT method of bioprinting is similar to ink-jet bioprinting and some bioplotting systems, in that LIFT printers deposit encapsulated cells in a dropwise, layer-by-layer manner onto a biopaper substrate. The key distinguishing feature of LIFT systems is that they employ a pulsed laser beam (1-100kHz) to cause the ejection of droplets, rather than a piezoelectric or thermal pulse [92,93]. In LIFT bioprinting, cells are encapsulated into a ribbon of a biocompatible medium, such as alginate, which is then affixed beneath a metallic absorption (ablator) layer. Directed pulsing of the laser source along the absorption layer causes focal point ablation, which induces vapor expansion above the cell-encapsulated film, which ultimately forces a droplet to be ejected onto the biopaper below [92].

4.2.5. Stereolithography

Stereolithography is a nozzleless fabrication technique that is able to generate cell-laden or non-cell bearing scaffolds by controlled beaming of directed light through a mirror array (or directly) into a bath of liquid, photocrosslinkable polymer resin or hydrogel. As each layer of the construct is photocrosslinked, the bath is lowered, and fresh resin is added [94]. In terms of printed construct resolution, stereolithography (SL) has been demonstrated to be one the most effective; reliably yielding submicron resolutions (0.43 μm) for acellular constructs [95] and 50μm for cell-laden ones [96]. SL largely relies on the integration of various photoinitiators, such as Irgacure 2959, LAP, VA-086, and eosin Y, to effectively crosslink the cell-bearing resin upon exposure to the directed light. As such, many stereolithography systems use light sources that project in the UV spectrum. Consequently, it well understood that UV light damages nucleic acids and can lead to cancerous growth, thus making UV light SL unfavorable for cell-laden bioinks. In order to circumnavigate this issue, our group employed a visible light projector and eosin y photocrosslinker (peak abs eosin y: λ = 510nm, green spectrum) integrated PEG-GelMA bioink to create a NIH 3T3 cell-laden construct, which displayed 85% cell viability 5 days post-printing [31]. An additional benefit of SL is the ability to integrate growth factors and nanoparticles into the cell-laden resin to effectively guide the differentiation of stem cell growth and promote cell proliferation [31,97].

4D stereolithographic printing relies on crosslinking a photocurable, polymeric resin or hydrogel with built-in shape-change propagating architectural features. These intrinsic shape-change directing features create internal stresses within the printed construct that make a given movement thermodynamically favorable when the printed construct is subjected to an initiation source such as electromagnetic radiation, heating/cooling, applied electrical current, or immersion in a solvent solution [33,35,36].

4.3. 3D bioprinting of neurological tissues and progress towards 4D studies

Due to the novel nature of 4D-bioprinting technology, the current literature pertaining to 4D bioprinting of neural tissues is very limited. Therefore, we will instead briefly outline a few recent advancements in 3D bioprinting of central nervous system/brain tissue studies to demonstrate the validity of the bioprinting approach for fabricating complex neural tissues as the field progresses towards a 4D-printed model in the future.

In their 2015 study, Lozano *et al.* used a custom-made, extrusion-based printer to fabricate a six- layer model of the cerebral cortex [28], illustrated by Figure 6. For their study, they developed a novel RGD-peptide-modified Gellan Gum (GG) bioink which encapsulated primary cortical neurons that had been excised from E-18 mice embryos. It was found that 5X DMEM and 1M calcium chloride could both be used to chemically cross-link the bioink in a manner that was non-harmful to the encapsulated cells. Additionally, it was found that at five days of continuous culture, there was no significant difference between the survivability of printed neural and glial cells between the printed constructs and the non-printed controls. The printed constructs were found to have diffusion coefficients for BSA 5.78×10^{-7} for GG and 5.15×10^{-7} for RGD-peptide GG. These results help to illustrate that the Gellan-gum hydrogels sufficiently promoted perfusion of proteinaceous compounds and nutrients in and out of the matrix. Moreover, researchers found that after five days of continuous culture, encapsulated neural cells continued to grow, divide, and form neural networks, extending axonal projections out of the cell-laden layers of the printed construct into the cell vacant layers, as shown in Figure 6 (d).

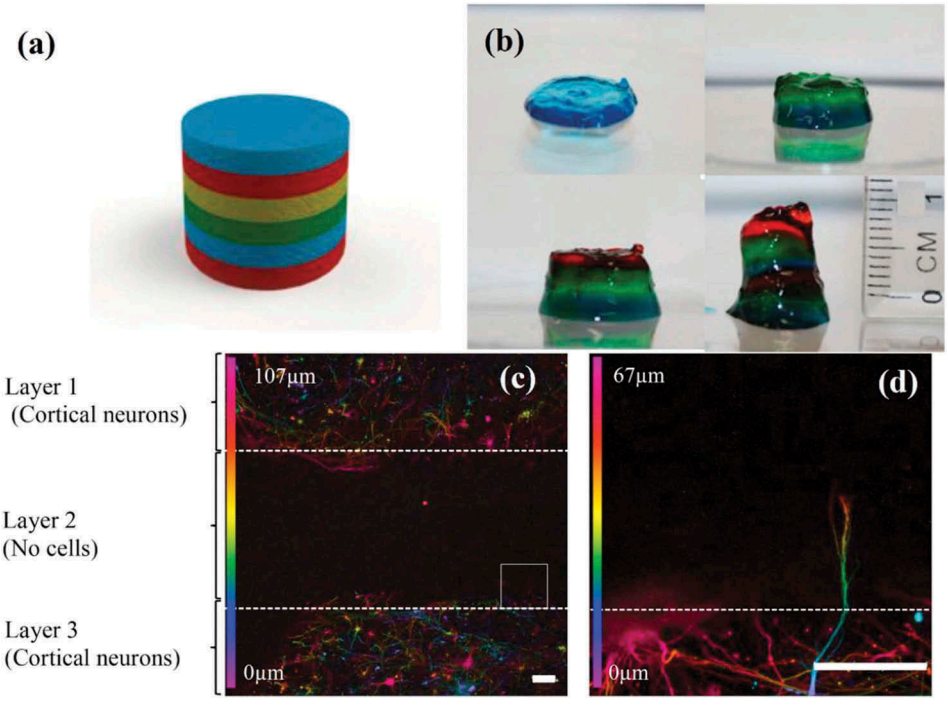

Figure 6. Extrusion-based bioprinted 6-layered model of the Cerebral cortex in RGD-peptide modified Gellan-gum (GG). (a) Solidworks design of 6-layered Cerebral cortex model. (b) Layer-by-layer extrusion printing of cortical model using RGD-peptide modified Gellan Gum as a bioink. (c) Distribution of printed cortical neurons throughout the layers of the construct. Construct layers alternate having incorporated cells or containing no cells. (d) Blow-out image of square area highlighted in (c) which shows an axonal projection penetrating into a cell-devoid layer. For (c) & (d), the scale bar is 100μm. Adapted with permission from [28].

In another recent study, a piezoelectric inkjet printer was used to test the survivability of rat retinal ganglion (RG) cells and glial cells throughout the printing process [32]. In a similar manner to the Lozano study, this study found that there was no significant difference in the survivability of RG cells and glial cells that were printed versus the non-printed control, even when drops were ejected at a repetition rate of 1 kHz at a speed of 13 m/s. Whereas it was found that there was cell loss in the printing process due to sedimentation within the printing apparatus itself, there does not appear to be a net effect on cell viability or retinal ganglion cell neurite extensions.

Interestingly, the work of Hsieh *et al.* 2015 showed that a thermosensitive murine NSC-laden hydrogel composed of water dispersed polyurethane (WDPU) nanoparticles, deemed 'PU2', was able to achieve stackable, post-print gelation at 37°C with considerable cell viability devoid of a crosslinking agent or harmful UV photoinitiation [98]. The PU2 bioink was generated by an aqueous synthesis process outlined by Hsu *et al.* 2014 [71], and was comprised of a > 65% soft segment portion. The soft segment portion of the bioink was synthesized using a 4:1 Molar ratio mixture of 2 synthetic diols: Poly(ε-capro-lactone) diol (PCL diol, M_n ~ 2000) as well as poly(D,L-lactide) diol (PDLLA diol, M_n ~2000), which had previously been demonstrated to exhibit highly tunable elasticity, biodegradability, and most importantly, general cytocompatibility. The PU2 bioink was subsequently formulated to 25% and 30% solid PU nanoparticle content in ink solution and loaded with promoter F1B-green florescence protein (F1B-GFP) transfected murine NSC's, labeled with PKH26 (Red fluorescent dye), at a cell density of 4×10^6 cells/ml. The cell-laden PU2 ink was then printed in a layered fashion to yield a 0.34 cm^3 construct upon a fused deposition manufacturing platform (FDM) mounted petri dish at 37°C (at a pressure of 55 kPa). Interestingly, post-printing inspection of PU2 print filament diameters showed that both the 25% and 30% PU2 solid component formulations saw a < 10 μm expansion 72 h after printing (d = 210μm at t = 0 h, d ≈ 220μm at t = 72 h). This minimal increase in printed fiber swelling seems to imply that PU2 is able to maintain relatively stable structural conformation upon printing devoid of a harsh chemical or photonic crosslinking mechanisms. Upon rheological analysis of both PU2 and its companion elastomer 'PU1', it was observed that PU2 25% had a modulus (G') of ~680 Pa while PU1 25% showed a modulus closer to 1.1 kPa, ~20-min post printing. This relatively low-observed G' of PU2 25% could have substantial implications for its potential utility as a hydrogel scaffold for *in vitro* brain tissue modeling, as it is notably similar to the purported elasticity modulus range of *in vivo* brain tissue. Whereas all other parameters were kept constant between the two PU 25% dispersions, it seems that the notable difference in the G' moduli between them is a function of the molecular differences between their secondary substituent diols. Both PU1 and PU2 had PCL as the primary diol in their formulations; however, PU1's secondary diol was Poly(L-lactide) diol (PLLA diol, M_n ~2000) as opposed to PDLLA diol as in PU2.

Recently, using our custom-made stereolithography printing platform, our lab successfully fabricated a 4D-printed graphene-enabled polymeric nerve guidance conduit which could be used for peripheral nervous system regeneration purposes, as well as for oriented guidance of stem cell growth [33], as is detailed in Figure 7. Human bone marrow mesenchymal stem cells (hMSCs) were shown to assume a highly aligned orientation on the 4D-bioprinted scaffolds. Interestingly, 4D-printed scaffolds also showed enhanced expression of the neurogenic factors ND1, NSE, and

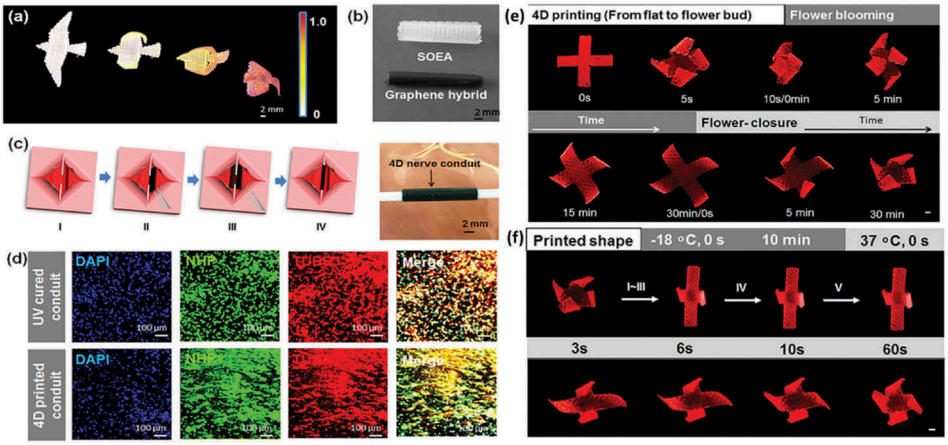

Figure 7. 4D bioprinting novel SOEA constructs. (a) Bird-like architectures fabricated from SOEA modified with graphene can achieve a 'flying' shape change by varying the graphene concentration (ranges tested 0–0.8%). (b) 4D bioprinted nerve guidance conduits with and without the addition of graphene. (c) Schematic of the self-entubulating nerve conduit being grafted onto the terminals of a damaged nerve (I-IV). The nerve conduit is placed over the damaged nerve stumps in its flattened temporary shape, but will fully cover the nerve in a self-entubulation/wrapping process at 37°C. Nerve damage model ensheathed by the 4D printed nanohybrid conduit. (d) Immunofluorescence staining of hMSCs cultured on both the nanohybrid and uv cured nerve conduits. The printed conduit demonstrated significantly greater cell alignment than the non-printed UV cured conduit. (e) Photo images of a reversible shape change process with 4D printed flower structure which can open in ethanol and close in water. (f) Beyond 4D printing – shape memory effect with the 4D printed flower structure. Scale bar, 2 mm. Adapted with permission from [33].

Ngn2 when compared to the controls. This data suggests that 4D-printed constructs can reliably enhance neurogenesis, while conferring desirable spatial characteristics (alignment) on the developing cells. As such, this same methodology for neural tissue engineering may in the future be extended to modeling radially aligned cortical cell-expansion. Furthermore, our study demonstrated that a unique laser-induced graded internal stress followed by a subsequent solvent-induced relaxation (Figure 7e) can drive a reversible and autonomous change of the programmed configuration after bioprinting. Moreover, the naturally derived shape memory polymer is able to trigger an additional 'thermomechanical programming' shape transformation over the 4D effect (Figure 7f).

5. Conclusions and future directions

Various computational and experimental studies have been conducted to model and elucidate the general mechanism which underlies the cortical folding process. In turn, it has been found that differential tangential expansion and migration of early neural cells in the developing cortex are mostly responsible for the buckling and folding that is observed. These and other studies have argued that it is mostly mechanical forces which guide cortical folding, but further experimentation should be conducted to verify these assertions. Moreover, additional attention should be devoted to

uncovering the effects that folding associated stresses, such as stretching, compressing, and varying stiffness, have on neural-cell fate commitment and terminal migration [63–66]. We expect that combinational 3D and 4D studies can be used to interrogate and verify the differential (tangential) growth pattern and axonal tension models as well as assess the effects of mechanical pressures on neuro-development. Particularly, the 4D-bioprinting approach is an excellent methodology by which to study the effects of cortical folding on stem cell proliferation and maturation because of the ease of experimental manipulation that it provides and its notable modifiability. Though 4D bioprinting is still in its respective infancy as a fabrication technique, we anticipate its rapid acceptance and expansion in the greater tissue engineering discipline in the years to come.

Disclosure statement

No potential conflict of interest was reported by the authors.

Funding

This work is supported by NSF MME program grant # 1642186, March of Dimes Foundation's Gene Discovery and Translational Research Grant and NIH Director's New Innovator Award 1DP2EB020549-01.

References

[1] E. Armstrong, A. Schleicher, H. Omran, M. Curtis, and K. Zilles, *The ontogeny of human gyrification*, Cereb. Cortex 5 (1) (1995), pp. 56–63. doi:10.1093/cercor/5.1.56.

[2] M. Sekiguchi, K. Shimai, M. Moriya, and R.S. Nowakowski, *Abnormalities of foliation and neuronal position in the cerebellum of NZB/BINJ mouse*, Dev. Brain Res. 64 (1991), pp. 189–195.

[3] G.L. Wallace, B. Robustelli, N. Dankner, L. Kenworthy, J.N. Giedd, and A. Martin, *Increased gyrification, but comparable surface area in adolescents with autism spectrum disorders*, Brain. 136 (6) (2013 Jun 1), pp. 1956–1967. ISSN 0006-8950. PMC 3673467 Freely accessible. PMID 23715094. doi:10.1093/brain/awt106

[4] T. Das, S. Borgwardt, D.J. Hauke, F. Harrisberger, U.E. Lang, A. Riecher-Rössler, L. Palaniyappan, and A. Schmidt, *Disorganized gyrification network properties during the transition to psychosis*, JAMA Psychiatry. 75(6) (2018), pp. 613–622. doi:10.1001/jamapsychiatry.2018.0391

[5] J.M. Harris, T.W.J. Moorhead, P. Miller, A.M. McIntosh, H.M. Bonnici, D.G.C. Owens, E. C. Johnstone, and S.M. Lawrie, *Increased prefrontal gyrification in a large high-risk cohort characterizes those who develop schizophrenia and reflects abnormal prefrontal development*, Biol. Psychiatry 62 (7) (2007), pp. 722–729. doi:10.1016/j.biopsych.2006.11.027.

[6] P. Nanda, N. Tandon, I.T. Mathew, C.I. Giakoumatos, H.A. Abhishekh, B.A. Clementz, G. D. Pearlson, J. Sweeney, C.A. Tamminga, and M.S. Keshavan, *Local gyrification index in probands with psychotic disorders and their first-degree relatives*, Biol. Psychiatry 76 (6) (2014), pp. 447–455. doi:10.1016/j.biopsych.2013.11.018.

[7] D. Essen and D. Essen, *A tension-based theory of morphogenesis and compact wiring in the central nervous system*, Nature. 385 (6614) (n.d.), pp. 313–318. doi:10.1038/385313a0

[8] B. Mota and S. Herculano-Houzel, *How the cortex gets its folds: An inside-out, connectivity-driven model for the scaling of mammalian cortical folding*, Front Neuroanat 6 (2012), pp. 3. doi:10.3389/fnana.2012.00003.

[9] J. Nie, L. Guo, G. Li, C. Faraco, L.S. Miller, and T. Liu, *A computational model of cerebral cortical folding*, J. Theor. Biol. 264 (2010), pp. 467–478. doi:10.1016/j.jtbi.2010.02.002.
[10] P.V. Bayly, R.J. Okamoto, G. Xu, Y. Shi, and L.A. Taber, *A cortical folding model incorporating stress-dependent growth explains gyral wavelengths and stress patterns in the developing brain*, Phys. Biol. 10 (1) (2013), pp. 016005. doi:10.1088/1478-3975/10/1/016005.
[11] L. Ronan, N. Voets, C. Rua, A. Alexander-Bloch, M. Hough, C. Mackay, T.J. Crow, A. James, J. N. Giedd, and P.C. Fletcher, *Differential tangential expansion as a mechanism for cortical gyrification*, Cereb. Cortex 24 (8) (2014), pp. 2219–2228. doi:10.1093/cercor/bht082.
[12] E. Lejeune, A. Javili, J. Weickenmeier, E. Kuhl, and C. Linder, *Tri-layer wrinkling as a mechanism for anchoring center initiation in the developing cerebellum*, Soft Matter 12 (25) (2016), pp. 5613–5620. doi:10.1039/c6sm00526h.
[13] C.D. Kroenke and P.V. Bayly, *How forces fold the cerebral cortex*, J. Neurosci. 38 (4) (2018), pp. 767. doi:10.1523/JNEUROSCI.0052-18.2018.
[14] V. Borrell, *How Cells Fold the Cerebral Cortex*, J. Neurosci. 38 (4) (2018), pp. 776–783. doi:10.1523/JNEUROSCI.1106-17.2017
[15] P.V. Bayly, L.A. Taber, and C.D. Kroenke, *Mechanical forces in cerebral cortical folding: A review of measurements and models*, J. Mech. Behav. Biomed. Mater. 29 (2014), pp. 568–581. doi:10.1016/j.jmbbm.2013.02.018.
[16] G. Striedter, S. Srinivasan, E. Monuki, and G. Striedter, *Cortical folding: when, where, how, and why?* Annu. Rev. Neurosci. 38 (n.d.), pp. 291. doi:10.1146/annurev-neuro-071714-034128.
[17] T. Tallinen, J.Y. Chung, J.S. Biggins, and L. Mahadevan, *Gyrification from constrained cortical expansion*, Proc. Nat. Acad. Sci. 111 (35) (2014), pp. 12667. doi:10.1073/pnas.1406015111.
[18] T. Tallinen, J.Y. Chung, F. Rousseau, N. Girard, J. Lefèvre, and L. Mahadevan, *On the growth and form of cortical convolutions*, Nat. Phys. 12 (2016), pp. 588. doi:10.1038/nphys3632.
[19] A. Thompson, E. Pillal, I. Dimov, S. Foster, C. Holt, and K. Franze, *Rapid changes in tissue mechanics regulate cell behavior in the developing embryonic brain*, eLife 8 (2019), pp. e39356. doi:10.7554/eLife.39356
[20] R. Stahl, T. Walcher, C. De Juan Romero, G. Pilz, S. Cappello, M. Irmler, J. Miguel Sanz-Aquela, J. Beckers, R. Blum, V. Borrell, and Götz, *Trnp1 regulates expansion and folding of the mammalian cerebral cortex by control of radial glial fate*, Cell 153 (3) (2013), pp. 535–549. doi:10.1016/j.cell.2013.03.027.
[21] M. Nonaka-Kinoshita, I. Reillo, B. Artegiani, M. Martínez-Martínez, M. Nelson, V. Borrell, and F. Calegari, *Regulation of cerebral cortex size and folding by expansion of basal progenitors*, Embo J. 32 (13) (2013), pp. 1817–1828. doi:10.1038/emboj.2013.96.
[22] I. Reillo, C.D.J. Romero, M.Á. García-Cabezas, and V. Borrell, *A role for intermediate radial glia in the tangential expansion of the mammalian cerebral cortex*, Cereb. Cortex 21(7) (2011, 1 July), pp. 1674–1694. doi:10.1093/cercor/bhq238.
[23] E. Legué, E. Riedel, and A.L. Joyner, *Clonal analysis reveals granule cell behaviors and compartmentalization that determine the folded morphology of the cerebellum*, Development 142 (9) (2015), pp. 1661. doi:10.1242/dev.120287.
[24] A. Sudarov and A.L. Joyner, *Cerebellum morphogenesis: The foliation pattern is orchestrated by multi-cellular anchoring centers*, Neural. Dev. 2 (2007), pp. 26. doi:10.1186/1749-8104-2-26.
[25] E. Karzbrun, A. Kshirsagar, S.R. Cohen, J.H. Hanna, and O. Reiner, *Human brain organoids on a chip reveal the physics of folding*, Nat. Phys. 14 (5) (2018), pp. 515–522. doi:10.1038/s41567-018-0046-7.
[26] B.G. Rash, S. Tomasi, H.D. Lim, C.Y. Suh, and F.M. Vaccarino, *Cortical gyrification induced by fibroblast growth factor 2 in the mouse brain*, J. Neurosci. 33 (26) (2013), pp. 10802–10814. doi:10.1523/JNEUROSCI.3621-12.2013
[27] R. Stahl, *Identification and functional analysis of Trnp1: A novel DNA associated protein with a key role in neurogenesis* (2012), pp. 86–88. https://edoc.ub.uni-muenchen.de/15432/.
[28] R. Lozano, L. Stevens, B.C. Thompson, K.J. Gilmore, R. Gorkin 3rd, E.M. Stewart, … G. G. Wallace, *3D printing of layered brain-like structures using peptide modified gellan gum substrates*, Biomaterials 67 (2015), pp. 264–273. doi:10.1016/j.biomaterials.2015.07.022

[29] Y.-B. Lee, S. Polio, W. Lee, G. Dai, L. Menon, R.S. Carroll, and -S.-S. Yoo, *Bio-printing of collagen and VEGF-releasing fibrin gel scaffolds for neural stem cell culture*, Exp. Neurol. 223 (2) (2010), pp. 645–652. doi:10.1016/j.expneurol.2010.02.014

[30] Q. Gu, E. Tomaskovic-Crook, R. Lozano, Y. Chen, R.M. Kapsa, Q. Zhou, … J.M. Crook, *Functional 3D neural mini-tissues from printed gel-based bioink and human neural stem cells*, Adv Healthc Mater. 5 (12) (2016), pp. 1429–1438. doi:10.1002/adhm.201600095

[31] S.J. Lee, W. Zhu, L. Heyburn, M. Nowicki, B. Harris, and L.G. Zhang, *Development of novel 3-D printed scaffolds with core-shell nanoparticles for nerve regeneration*, IEEE Trans. Biomed. Eng. 64 (2) (2017), pp. 408–418. doi:10.1109/TBME.2016.2558493

[32] B. Lorber, W.-K. Hsiao, I.M. Hutchings, and K.R. Martin, *Adult rat retinal ganglion cells and glia can be printed by piezoelectric inkjet printing*, Biofabrication 6 (1) (2014), pp. 015001. doi:10.1088/1758-5082/6/1/015001.

[33] S. Miao, et al. *Stereolithographic 4D bioprinting of multiresponsive architectures for neural engineering*, Adv. Biosys. 2 (9) (2018), pp. 1800101. doi:10.1002/adbi.201800101

[34] S. Miao, W. Zhu, N. Castro, M. Nowicki, H. Cui, X. Zhou, J.P. Fisher, and L.G. Zhang, *4D printing smart biomedical scaffolds with novel soybean oil epoxidized acrylate*, Sci. Rep. 6 (2016), pp. 27226. doi:10.1038/srep27226.

[35] S. Miao, H. Cui, M. Nowicki, S. Lee, J. Almeida, X. Zhou, W. Zhu, X. Yao, F. Masood, M. Plesniak, M. Mohiuddin, and L.G. Zhang, *Photolithographic-stereolithographic-tandem fabrication of 4D smart scaffolds for improved stem cell cardiomyogenic differentiation*, Biofabrication 10 (3) (2018), pp. 035007. doi:10.1088/1758-5090/aabe0b.

[36] S. Miao, N. Castro, M. Nowicki, L. Xia, H. Cui, X. Zhou, W. Zhu, S.-J. Lee, K. Sarkar, G. Vozzi, Y. Tabata, J. Fisher, and L.G. Zhang, *4D printing of polymeric materials for tissue and organ regeneration*, Mater. Today 20 (10) (2017), pp. 577–591. doi:10.1016/j.mattod.2017.06.005.

[37] A. Sydney Gladman, E.A. Matsumoto, R.G. Nuzzo, L. Mahadevan, and J.A. Lewis, *Biomimetic 4D printing*, Nat. Mater. 15 (4) (2016), pp. 413–418. doi:10.1038/nmat4544.

[38] X. Zhou, H. Cui, M. Nowicki, S. Miao, S.J. Lee, F. Masood, B. Harris, and L.G. Zhang, *3D bioprinted dopamine based matrix for promoting neural regeneration*, ACS Appl. Mater. Interfaces 10 (10) (2018), pp. 8993–9001. doi:10.1021/acsami.7b18197.

[39] S. Lee, W. Zhu, M. Nowicki, G. Lee, D.N. Heo, J. Kim, Y. Zuo, and L.G. Zhang, *3D printing nano conductive multi-walled carbon nanotube scaffolds for nerve regeneration*, J. Neural Eng. 15 (2018), pp. 016018. doi:10.1088/1741-2552/aa95a5.

[40] W. Zhu, T. Ye, S.J. Lee, H. Cui, S. Miao, X. Zhou, D. Shuai, and L.G. Zhang, *Enhanced neural stem cell functions in conductive annealed carbon nanofibrous scaffolds with electrical stimulation*, Nanomed. Nanotech. Biol. Med. 14(7) (2018), pp. 2485–2494. doi:10.1016/j.nano.2017.03.018

[41] W. Zhu, J.K. George, V. Sorger, and L.G. Zhang, *3D printing scaffold coupled with low level light therapy for neural tissue regeneration*, Biofabrication 9 (2017), pp. 025002. doi:10.1088/1758-5090/aa6999.

[42] S. Lee, M. Nowicki, B. Harris, and L.G. Zhang, *Fabrication of a highly aligned neural scaffold via a table top stereolithography 3D printing and electrospinning*, Tissue Eng. Part A 23 (11–12) (2017), pp. 491–502. doi:10.1089/ten.TEA.2016.0353.

[43] W. Zhu, F. Masood, J. O'Brien, and L.G. Zhang, *Highly aligned nanocomposite scaffolds by electrospinning and electrospraying for neural tissue regeneration*, Nanomed. Nanotech. Biol. Med. 11 (3) (2015), pp. 693–704. doi:10.1016/j.nano.2014.12.001.

[44] S. Miao, W. Zhu, N. Castro, J.S. Leng, and L.G. Zhang, *4D printing hierarchy scaffolds with highly biocompatible smart polymers for tissue engineering applications*, Tissue Eng.Part C 22 (10) (2016), pp. 952–963. doi:10.1089/ten.tec.2015.0542.

[45] M.L. Shuler and J.J. Hickman, *Toward in vitro models of brain structure and function*, Proc. Nat. Acad. Sci. 111(38) (2014), pp. 13682–13683. doi:10.1073/pnas.1414484111

[46] A. Parent, *Carpenter's human neuroanatomy* (1996). (9)P-25, P-38, P421-463, P469-519, P527-572 P583-623 P633-694 P706-738 P769-773

[47] F.A. Azevedo, L.R. Carvalho, L.T. Grinberg, J.M. Farfel, R.E. Ferretti, R.E. Leite, … S. Herculano-Houzel, *Equal numbers of neuronal and nonneuronal cells make the human brain an isometrically scaled-up primate brain*, J. Comp. Neurol. 513 (5) (2009), pp. 532–541. doi:10.1002/cne.21974

[48] T. Vanderah and D. Gould, *Nolte's the Human Brain: An Introduction to Its Functional Anatomy*, Vol. 7, Elsevier, Inc, Philadelphia (2016), pp. P77. ISBN-13:978-1455728596

[49] E. Mancall and D. Brock *Gray's clinical neuroanatomy: the anatomical basis for clinical neuroscience* (2011), pp. P308.

[50] R. Snell, *Clin. Neuroanat. edition7*, *Ch 6 The Cerebellum and its Connections, Ch. 7 The Cerebrum*, Lippincott Williams & Wilkins, Philadelphia (2010), pp.P252–270.

[51] H. Blumenfeld, *Neuroanatomy through Clinical Cases*, 2nded, Sinauer Associates, Sunderland, Mass., pp. 21, 2010, ISBN 9780878936137. Areas of the CNS made up mainly of myelinated axons are called white matter.

[52] S. Standring, *Gray's anatomy: the anatomical basis of clinical practice*, 41, Elsevier, Inc, New York (2016), pp. P287, P228-229, 279–280. ISBN:9780702052309

[53] K. Brodmann and L. Garey, *Brodmann's localisation in the cerebral cortex: the prinicples of comparative localisation in the cerebral cortex based on cytoarchitectures* (1994), pp. 3

[54] O. Oscarsson, *Spatial distribution of climbing and mossy fibre inputs in the cerebellar cortex. ID*, in *Afferent and Intrinsic Organization of Laminated Structures in the Brain*, O. Creutzfeldt, ed., Springer-Verlag, Berlin, 1976, pp. 34–42.

[55] M. Ito, *Cerebellar circuitry as a neuronal machine*, Prog. Neurobiol. 78 (3) (2006), pp. 272–303. doi:10.1016/j.pneurobio.2006.02.006.

[56] R.R. Llinas, K.D. Walton, and E.J. Lang, *Ch. 7 cerebellum*, in *The Synaptic Organization of the Brain*, G.M. Shepherd, ed., Oxford University Press, New York, 2004. pp. 271–309. ISBN 13: 9780195159561

[57] B. Fischl and A.M. Dale, *Measuring the thickness of the human cerebral cortex from magnetic resonance images*, Proc. Nat. Acad. Sci. 97 (20) (2000), pp. 11050. doi:10.1073/pnas.200033797.

[58] E. Gheorghe, S. Vameşu, V. Tomuta, M. Hîncu, T. Mehedinţi, and G. Nicola, *Cerebellar atrophy–A comparative microscopic study*, Rom. J. Morphol. Embryol. 47 (2006), pp. 345349.

[59] D. Barry, J. Pakan, and K. McDermott. *Radial glial cells: Key organisers in CNS development*, International Journal of Biochemistry & Cell Biology. 46 (2014). pp. 76–79

[60] C.C. Hilgetag and H. Barbas, *Role of mechanical factors in the morphology of the primate cerebral cortex*, PLoS Comput. Biol. 2 (3) (2006), pp. e22. doi:10.1371/journal.pcbi.0020022.

[61] G. Xu, A.K. Knutsen, K. Dikranian, C.D. Kroenke, P.V. Bayly, and L.A. Taber, *Axons pull on the brain, but tension does not drive cortical folding*, ASME. J Biomech. Eng. 132(7) (2010), pp. 071013–071013-8. doi:10.1115/1.4001683

[62] D.P. Richman, R.M. Stewart, J.W. Hutchinson, and V.S. Caviness, *Mechanical model of brain convolution development,* Science 189 (1975), pp. 18–21. doi:10.1126/science.1135626.

[63] Y.J. Chang, C.J. Tsai, F.G. Tseng, T.J. Chen, and T.W. Wang, *Micropatterned stretching system for the investigation of mechanical tension on neural stem cells behavior*, Nanomedicine 9(3) (2013, Apr), pp. 345–355. doi:10.1016/j.nano.2012.07.008.

[64] D.E. Koser, A.J. Thompson, S.K. Foster, A. Dwivedy, E.K. Pillai, G.K. Sheridan, H. Svoboda, M. Viana, L.D. Costa, J. Guck, C.E. Holt, and K. Franze, *Mechanosensing is critical for axon growth in the developing brain*, Nat. Neurosci. 19(12) (2016, Dec), pp. 1592–1598. doi:10.1038/nn.4394. Epub 2016 Sep 19. PubMed PMID: 27643431; PubMed Central PMCID: PMC5531257.

[65] E.H. Barriga, K. Franze, G. Charras, and R. Mayor, *Tissue stiffening coordinates morphogenesis by triggering collective cell migration in vivo*, Nature 554 (2018), pp. 523. doi:10.1038/nature25742.

[66] J. Arulmoli, M.M. Pathak, L.P. McDonnell, J.L. Nourse, F. Tombola, J.C. Earthman, and L. A. Flanagan, *Static stretch affects neural stem cell differentiation in an extracellular matrix-dependent manner*, Sci. Rep. 5 (2015), pp. 8499. doi:10.1038/srep08499.

[67] Q. Ge, A.H. Sakhaei, H. Lee, C.K. Dunn, N.X. Fang, and M.L. Dunn, *Multimaterial 4D printing with tailorable shape memory polymers*, Sci. Reports (Nature Publisher Group) 6 (08) (2016), pp. 31110. doi:10.1038/srep31110.

[68] P. Morouço, W. Lattanzi, and N. Alves, *Four-dimensional bioprinting as a new era for tissue engineering and regenerative medicine*, Frontiers Bioeng. Biotechnol. 5 (2017), pp. 61. doi:10.3389/fbioe.2017.00061.

[69] D. Raviv, W. Zhao, C. McKnelly, A. Papadopoulou, A. Kadambi, S. Hirsch, D. Dikovsky, M. Zyracki, C. Olguin, R. Raskar, and S. Tibbits, *Active printed materials for complex self-evolving deformations*, Sci. Rep. 4 (2014), pp. 7422. doi:10.1038/srep07422.

[70] A. Banerjee, M. Arha, S. Choudhary, R.S. Ashton, S.R. Bhatia, D.V. Schaffer, and R.S. Kane, *The influence of hydrogel modulus on the proliferation and differentiation of encapsulated neural stem cells*, Biomaterials 30 (27) (2009), pp. 4695–4699. doi:10.1016/j.biomaterials.2009.05.050.

[71] S.-H. Hsu, K.-C. Hung, -Y.-Y. Lin, C.-H. Su, H.-Y. Yeh, U.S. Jeng, … J.-C. Lin, *Water-based synthesis and processing of novel biodegradable elastomers for medical applications*, J. Mater. Chem. B. 2 (31) (2014), pp. 5083–5092. doi:10.1039/C4TB00572D

[72] E. Yang, S. Miao, J. Zhong, Z. Zhang, D.K. Mills, and L.G. Zhang, *Bio-based polymers for 3D printing of bioscaffolds*, Polymer Reviews (2018). doi:10.1080/15583724.2018.1484761.

[73] J.A. Phillippi, E. Miller, L. Weiss, J. Huard, A. Waggoner, and P. Campbell, *Microenvironments engineered by inkjet bioprinting spatially direct adult stem cells toward muscle- and bone-like subpopulations*, Stem Cells. 26 (1) (2008), pp. 127–134. doi:10.1634/stemcells.2007-0520

[74] C.M. O'Brien, B. Holmes, S. Faucett, and L.G. Zhang, *Three-dimensional printing of nanomaterial scaffolds for complex tissue regeneration*, Tissue Eng. Part B Rev. 21 (1) (2015), pp. 103–114. doi:10.1089/ten.TEB.2014.0168

[75] S.V. Murphy and A. Atala, *3D bioprinting of tissues and organs*, Nat. Biotechnol. 32 (8) (2014), pp. 773–785. doi:10.1038/nbt.2958

[76] Q. Zheng, J. Lu, H. Chen, L. Huang, J. Cai, and Z. Xu, *Application of inkjet printing technique for biological material delivery and antimicrobial assays*, Anal. Biochem. 410 (2) (2011), pp. 171–176. doi:10.1016/j.ab.2010.10.024

[77] T. Xu, J. Jin, C. Gregory, J.J. Hickman, and T. Boland, *Inkjet printing of viable mammalian cells*, Biomaterials. 26 (1) (2005), pp. 93–99. doi:10.1016/j.biomaterials.2004.04.011

[78] X. Cui, D. Dean, Z.M. Ruggeri, and T. Boland, *Cell damage evaluation of thermal inkjet printed Chinese hamster ovary cells*, Biotechnol. Bioeng. 106 (6) (2010), pp. 963–969. doi:10.1002/bit.22762

[79] T. Xu, W. Zhao, J.-M. Zhu, M.Z. Albanna, J.J. Yoo, and A. Atala, *Complex heterogeneous tissue constructs containing multiple cell types prepared by inkjet printing technology*, Biomaterials. 34 (1) (2013), pp. 130–139. doi:10.1016/j.biomaterials.2012.09.035

[80] W. Jia, P.S. Gungor-Ozkerim, Y.S. Zhang, K. Yue, K. Zhu, W. Liu, … A. Khademhosseini, *Direct 3D bioprinting of perfusable vascular constructs using a blend bioink*, Biomaterials 106 (2016), pp. 58–68. doi:10.1016/j.biomaterials.2016.07.038

[81] L. Ouyang, R. Yao, Y. Zhao, and W. Sun, *Effect of bioink properties on printability and cell viability for 3D bioplotting of embryonic stem cells*, Biofabrication. 8 (3) (2016), pp. 035020. doi:10.1088/1758-5090/8/3/035020

[82] D.W. Hutmacher, T. Schantz, I. Zein, K.W. Ng, S.H. Teoh, and K.C. Tan, *Mechanical properties and cell cultural response of polycaprolactone scaffolds designed and fabricated via fused deposition modeling*, J. Biomed. Mater. Res. 55 (2001), pp. 203–216. doi:10.1002/1097-4636(200105)55:2<203::AID-JBM1007>3.0.CO;2-7

[83] S. Ji and M. Guvendiren, *Recent advances in bioink design for 3D bioprinting of tissues and organs*, Frontiers Bioeng. Biotechnol. 5 (2017), pp. 23. doi:10.3389/fbioe.2017.00023

[84] D.T. Pham and R.S. Gault, *A comparison of rapid prototyping technologies*, Int. J. Mach. Tools Manufacture. 38 (10) (1998), pp. 1257–1287. doi:10.1016/S0890-6955(97)00137-5

[85] T. Pan, W. Song, X. Cao, and Y. Wang, *3D bioplotting of gelatin/alginate scaffolds for tissue engineering: influence of crosslinking degree and pore architecture on physicochemical properties*, J. Mater. Sci. Technol. 32 (9) (2016), pp. 889–900. doi:10.1016/j.jmst.2016.01.007

[86] Q. Gu, E. Tomaskovic-Crook, G.G. Wallace, and J.M. Crook, *3D bioprinting human induced pluripotent stem cell constructs for in situ cell proliferation and successive multilineage differentiation*, Adv Healthc Mater 6 (2017), pp. 17. doi:10.1002/adhm.201700175

[87] R.L. Simpson, F.E. Wiria, A.A. Amis, C.K. Chua, K.F. Leong, U.N. Hansen, M. Chandrasekaran, and M.W. Lee, *Development of a 95/5 poly(L-lactide-co-glycolide)/hydroxylapatite and β-tricalcium phosphate scaffold as bone replacement material via selective laser sintering*, J. Biomed. Mater. Res. 84B (2008), pp. 17–25. doi:10.1002/jbm.b.30839

[88] S. Das, S.J. Hollister, C. Flanagan, A. Adewunmi, K. Bark, C. Chen, K. Ramaswamy, D. Rose, and E. Widjaja, *Freeform fabrication of nylon-6 tissue engineering scaffolds*, Rapid Prototyping J. 9 (2003), pp. 43–49. doi:10.1108/13552540310455656.

[89] J.M. Williams, A. Adewunmi, R.M. Schek, C.L. Flanagan, P.H. Krebsbach, S.E. Feinberg, S. J. Hollister, and S. Das, *Bone tissue engineering using polycaprolactone scaffolds fabricated via selective laser sintering*, Biomaterials 26 (2005), pp. 4817–4827. doi:10.1016/j.biomaterials.2004.11.057.

[90] C.K. Chua, K.F. Leong, K.H. Tan, F.E. Wiria, and C.M. Cheah, *Development of tissue scaffolds using selective laser sintering of polyvinyl alcohol/hydroxyapatite biocomposite for craniofacial and joint defects*, J. Mater. Sci. Mater. Med. 15 (2004), pp. 1113–1121.

[91] F.E. Wiria, K.F. Leong, C.K. Chua, and Y. Liu, *Poly-ε-caprolactone/hydroxyapatite for tissue enginering scaffold fabrication via selective laser sintering*, Acta. Biomater. 3 (2007), pp. 1–12. doi:10.1016/j.actbio.2006.07.008.

[92] C. Mézel, A. Souquet, L. Hallo, and F. Guillemot. *Bioprinting by laser-induced forward transfer for tissue engineering applications: Jet formation modeling,* Biofabrication 2 (2010), pp. 014103. doi:10.1088/1758-5082/2/1/014103.

[93] F. Guillemot, A. Souquet, S. Catros, B. Guillotin, J. Lopez, M. Faucon, … J. Amédée, *High-Throughput Laser Printing of Cells and Biomaterials for Tissue Engineering*, *Acta Biomaterialia*. 6(7) 2009. doi:10.1016/j.actbio.2009.09.029

[94] F.P.W. Melchels, J. Feijen, and D.W. Grijpma, *A review on stereolithography and its applications in biomedical engineering*, Biomaterials. 31 (24) (2010), pp. 6121–6130. doi:10.1016/j.biomaterials.2010.04.050

[95] S. Maruo and K. Ikuta, *Submicron stereolithography for the production of freely movable mechanisms by using single-photon polymerization*, Sensors Actuators A: Phys. 100 (1) (2002), pp. 70–76. doi:10.1016/S0924-4247(02)00043-2

[96] Z. Wang, R. Abdulla, B. Parker, R. Samanipour, S. Ghosh, and K. Kim, *A simple and high-resolution stereolithography-based 3D bioprinting system using visible light crosslinkable bioinks*, Biofabrication 7 (4) (2015), pp. 045009. doi:10.1088/1758-5090/7/4/045009.

[97] O. Guillaume, M.A. Geven, C.M. Sprecher, V.A. Stadelmann, D.W. Grijpma, T.T. Tang, … D. Eglin, *Surface-enrichment with hydroxyapatite nanoparticles in stereolithography-fabricated composite polymer scaffolds promotes bone repair*, Acta. Biomater. 54 (2017), pp. 386–398. doi:10.1016/j.actbio.2017.03.006

[98] F.-Y. Hsieh, -H.-H. Lin, and S.-H. Hsu, *3D bioprinting of neural stem cell-laden thermoresponsive biodegradable polyurethane hydrogel and potential in central nervous system repair*, Biomaterials. 71 (SupplementC) (2015), pp. 48–57. doi:10.1016/j.biomaterials.2015.08.028